Multistage Time-Optimal Control for Synchronization Process in Electric-Driven Mechanical Transmission With Angle Alignment Considering Torque Response Process

Ziwang Lu[1]
State Key Laboratory of Automotive Safety and Energy,
School of Vehicle and Mobility,
Tsinghua University,
Beijing 100084, China
e-mail: luzw1992@gmail.com

Guangyu Tian
Professor
State Key Laboratory of Automotive Safety and Energy,
School of Vehicle and Mobility,
Tsinghua University,
Beijing 100084, China
e-mail: tian_gy@tsinghua.edu.cn

Simona Onori
Professor
Mem. ASME
Department of Energy Resources Engineering,
Stanford University,
Stanford, CA 94305
e-mail: sonori@stanford.edu

The synchronization process takes up almost one half of the time of the gear-shifting process, and also influences the impacts between the sleeve and the gear ring. To avoid impacts and reduce time duration, a time-optimal control strategy with angle alignment is necessary for the synchronization process. Moreover, to be better accord with practice, the motor torque response process should be taken into account. The parameters in the torque response process depend on control commands, which makes the control problem a multistage one. To solve these issues, a rule-based control strategy is extracted from the dynamic programming (DP) solution of the multistage time-optimal control problem. To obtain this strategy, the dynamic model for the synchronization process with a modified Sigmoid model to precisely depict the torque response process is first solved. Then, the control problem is formulated as a multistage time-optimal control problem with three states and solved by DP. Based on the DP results, a three-stage and a four-stage rule-based control strategies are extracted for normal operation situation and startup situation, respectively. Finally, through comparative studies, the proposed rule-based control strategy can eliminate the speed difference and angle difference simultaneously with almost the same time of the bang–bang control, while the bang–bang control cannot obtain the zero terminals. Moreover, the proposed control strategy only takes 20 ms more than the pure speed synchronization control in the worst case. It would decrease when the initial speed difference increases. [DOI: 10.1115/1.4048783]

1 Introduction

Electric vehicles (EVs) attract extensive attention of the world due to the increasing fossil fuel price and the increasingly strict emission regulations, and are developed rapidly with the technical development of the electric motor and the battery [1,2]. However, electric motors have their torque limitation and low-efficiency regions. Equipped with a transmission, electric vehicles can not only extend the drive force range but also optimize the working point of the drive motor by changing the gear [3–5].

With high transmission efficiency, low cost, simple mechanical structure, and the ability for different-size vehicles, an automated manual transmission (AMT) is a suitable choice for EVs [5]. Moreover, the drive motor can be directly integrated with the AMT without a clutch between them since the drive motor can start at zero speed. By eliminating the complicated clutch system, we can save both weight and the cost of the powertrain. We call this system the clutchless automated manual transmission (CLAMT), shown in Fig. 1(*a*). However, there exists shift jerk and long torque interruption during the gear-shifting process, which would reduce the vehicles' dynamic performance as well as drivability.

During the gear-shifting process, the sleeve disengages from the original gear ring, travels through the neutral clearance, and then engage with the target gear ring. Detailed mechanical diagram is shown in Fig. 1(*b*) or 1(*d*). Given an instance from the second gear to the first gear, the sleeve originally engages with the second gear ring. The corresponding power transmission routes are shown in Fig. 2(*a*). After the gear-shifting process, the sleeve would engage with the first gear ring. The corresponding power transmission routes are shown in Fig. 2(*b*). During the process, the power from the drive motor cannot be transmitted to the vehicle due to the disengagement of the sleeve and the gear ring. Therefore, we expect this process to end as soon as possible. According to the transmission routes in Fig. 2, the sleeve has the same speed of the second gear ring after the disengagement, which is obviously different from that of the target gear ring, namely, the first gear ring. The speed difference between the sleeve and the target gear ring should be reduced to near zero before the engagement to avoid or decline the impacts between them, otherwise the teeth on the sleeve and gear ring, shown in Fig. 1(*b*) or 1(*d*), would bump against each other, resulting in shift jerk or shock. The process of reducing the speed difference is called the synchronization process. It takes up most of the time duration of the gear-shifting process and determines the level of the shift jerk. Therefore, the synchronization process plays an essential role in the gear-shifting process.

Researchers on the synchronization process can be divided into two groups according to the mechanical structure differences. The first group focuses on the CLAMT with a synchronizer, shown in Fig. 1(*a*), and the second group aims at the system without a synchronizer, shown in Fig. 1(*c*). The synchronizer, shown in Fig. 1(*b*), is a significant component to accelerate the synchronization process by the cone friction between the sychronizer and the gear ring [6]. In general, the speed difference is reduced first by the

[1]Corresponding author.

Contributed by the Dynamic Systems Division of ASME for publication in the Journal of Dynamic Systems, Measurement, and Control. Manuscript received June 8, 2020; final manuscript received October 4, 2020; published online November 4, 2020. Assoc. Editor: Scott Moura.

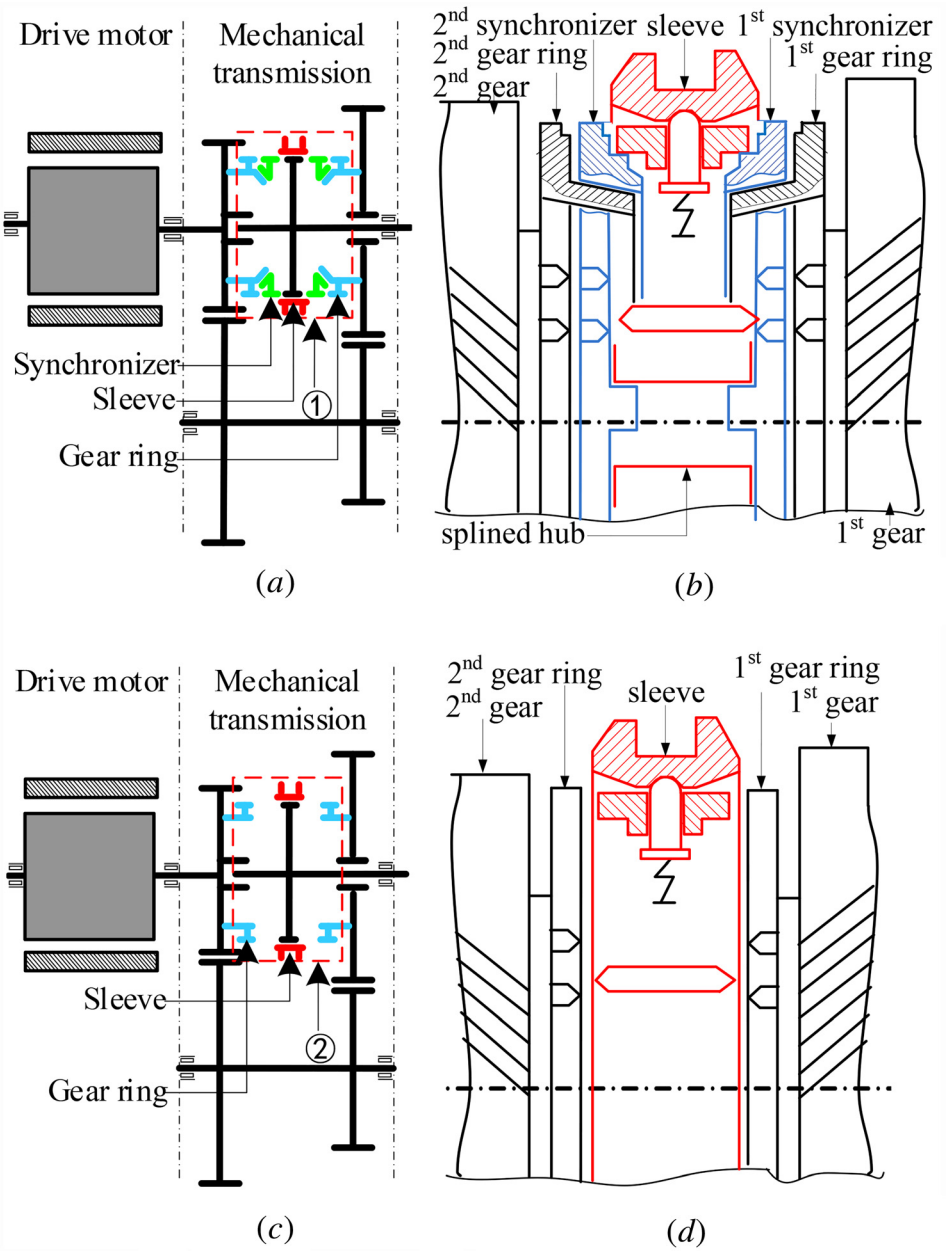

Fig. 1 Mechanical diagram of CLAMT and EMT: (*a*) CLAMT, (*b*) detailed structure of ① in (*a*), (*c*) EMT, and (*d*) detailed structure of ② in (*b*)

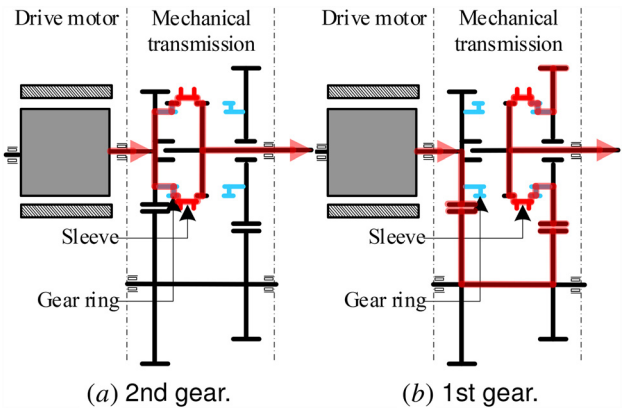

Fig. 2 Mechanical power transmission routes. The routes are shaded in red: (*a*) second gear and (*b*) first gear.

active synchronization of the drive motor, then eliminated completely through the cone friction. Previous research pays more attention to the dynamic model of the synchronization process [7–9]. A continuous model is utilized to depict the interaction between the sleeve and the synchronizer in Ref. [7], while a discrete model applied in Refs. [8] and [9]. Besides the synchronizer model, research on the active synchronization control to accelerate the synchronization process by adjusting the drive motor torque is also strongly pursued. A dual sliding control is applied to reduce the response time and static error of the rotational speed of the drive motor in Ref. [10]. The shortest shifting time is approximately 600 ms, which is validated on a bench test. The effect of the final rotational speed difference between the sleeve and the gear ring on active synchronization time is analyzed in Ref. [11]. The results indicate that the active synchronization time decreases when the final speed difference increases. The terminal speed difference is limited below 10 rpm in Ref. [12]. The shifting process takes less than 1500 ms, with the shifting jerk less than 15 m/s^3. In

Refs. [13] and [14], a sliding control is applied to adjust the speed of the drive motor and validate that algorithm by tests on a shifting test rig. According to the results, the up-shift time and down-shift time are almost 2440 ms and 1590 ms, respectively. In Ref. [15], a proportional feedback controller extracted from the linear quadratic regulator with a disturbance observer is designed to synchronize the speed. The control strategy can be implemented online and take about 800 ms to complete the synchronization process. Some researchers also focus on designing novel synchronization mechanics, a Harpoon-shift synchronizer is proposed in Refs. [16] and [17]. It can reduce the impacts to some extent but cannot eliminate them.

As far as the CLAMT without a synchronizer, we call this system the electric-driven mechanical transmission (EMT) since only the electric motor is involved in the synchronization process. In Ref. [18], the synchronizer is removed from the transmission, and the feasibility is validated in a conventional vehicle with an internal combustion engine (ICE). After that, less research focuses on the nonsynchronizer mechanical transmission due to the vibration out of the rough control of the ICE. In the last decade, the EMT attracts the attention of the researchers again with the development of EVs since the electric motor has more precise and fast control ability. In Ref. [19], the dynamic model for the engaging process is built based on a EMT of heavy-duty vehicles. It indicates that it should be a better choice to choose the minimal rotation speed difference at the same gear-shifting success ratio. In Refs. [20] and [21], a more precise impact model between the sleeve and the gear ring is proposed to capture the trajectory of the components, which can facilitate designing control strategy. In Ref. [22], the terminal speed difference is declined to nearly zero using the speed mode embedded in the motor controller unit (MCU) with a shifting time of about 890 ms, but impacts still exist. These days researchers claim that not only the speed difference but the angle difference between the sleeve and the gear ring has a significant influence on the impact between the two components [23–26]. It is evident that if there is no speed difference and no angle difference between the sleeve and the gear ring, the impacts would be eliminated. That means synchronizing the speed difference meanwhile aligning the angle difference between the sleeve and gear ring, which we call dual synchronization. To reduce the time during the synchronization process, a theoretical time-optimal control law of dual synchronization based on the Pontryagin's minimum principle (PMP) is solved in Refs. [23] and [26]. In Ref. [24], an empirical dual synchronization optimal strategy is proposed to eliminate the speed and angle difference.

As stated above, a CLAMT with a synchronizer not only removes the complex clutch system but accelerates the speed synchronization through the active synchronization of the electric motor. Previous research on the CLAMT pays more attention to the active speed synchronization control. By removing the synchronizer from the CLAMT, the EMT makes the dual synchronization achievable to eliminate impacts between the sleeve and the gear ring. Previous research on EMTs concentrates on relationships among the speed difference, gear-shifting success ratio, and gear-shifting time. To obtain the time-optimal dual synchronization for the EMT, an empirical control law and a theoretical time-optimal control law are resolved in Refs. [23] and [24], respectively. However, the torque response process of the drive motor is ignored in both cases, which would result in impacts.

We derive a rule-based control strategy, which is extracted from the results of dynamic programming (DP) and easily applied to practice. The torque response process is taken into account to obtain the strategy. Therefore, the proposed strategy can achieve zero speed difference and angle difference, which can eliminate the impacts. First, to better depict the torque trajectory during the torque response process, we propose a modified Sigmoid model. Unlike the simple first-order motor model, the parameters in the proposed model are coupled with the torque command, which makes the optimal control problem a multistage one. To solve the optimal control law with dynamic programming, the motor torque is introduced as another state to satisfy the nonaftereffect property. Therefore, there are three states in this control problem, the motor torque, the speed difference and the angle difference. Moreover, for practical application, an online rule-based control strategy is derived from the results of DP inspired by Biasini et al. [27].

The paper is organized as follows. Section 2 presents the mechanical and control diagram of the EMT. The dynamic model for the synchronization process with a modified Sigmoid model during the torque response process is derived in Sec. 3. Then, the control problem is formulated as a multistage time-optimal one with three states in Sec. 4. After that, the solution procedure based on DP is presented in Sec. 5. The rules are extracted in Sec. 6. Section 7 conducts comparative studies with the bang–bang control and pure speed synchronization control. Finally, Sec. 8 summarizes the conclusions and proposes the future work.

2 System Description

As shown in Fig. 3, the EMT consists of one drive motor, one mechanical transmission without synchronizers, and an angular sensor on the output shaft. The output shaft connects to the wheel through the final drive. The rotor of the drive motor is directly connected to the input shaft of the transmission. In the transmission, the rotational motions of the first gear and the second gear is transmitted from the drive motor through the gear transmission. That means

$$\theta_{\mathrm{gr}} = \frac{\theta_m}{i_g}$$
$$\omega_{\mathrm{gr}} = \frac{\omega_m}{i_g} \tag{1}$$

where θ_m and ω_m denote the rotational angle and speed of the drive motor, respectively, θ_{gr} and ω_{gr} denote the rotational angle and speed of the gear ring, respectively, and i_g is the transmission ratio of the desired gear. The sleeve is connected with the output shaft directly. Therefore, the angular sensor installed on the output shaft of the transmission can capture the rotational angle θ_{slv} of the sleeve.

As far as the control diagram in Fig. 4, the control system consists of one transmission control unit (TCU), one MCU, and the plant EMT. The TCU calculates and transmits the torque command T_{cmd} of the drive motor to the MCU. The torque command is determined according to the rotational angle θ_{slv} of the sleeve from the angular sensor, the angle θ_m, speed ω_m and the estimated torque $\hat{T}_m$ of the drive motor from the MCU. The MCU determines the three-phase current according to the build-in control algorithm. The control algorithm is unknown to users.

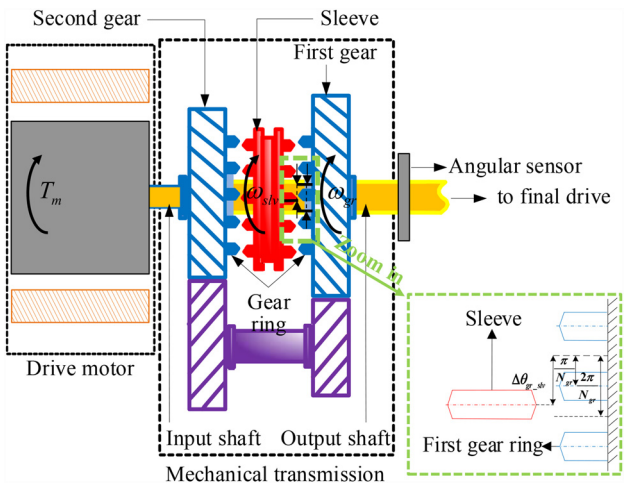

Fig. 3 Mechanical system diagram

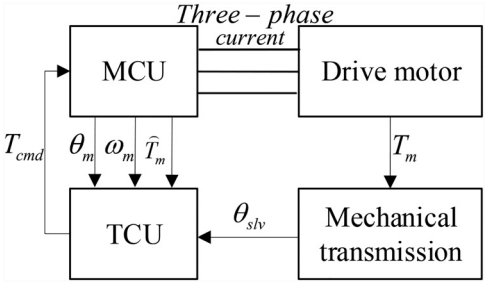

Fig. 4 Control system diagram. MCU is the abbreviation of motor control unit. TCU is the abbreviation of TCU.

3 System Model

The dynamic model for the synchronization process is built herein. Traditional synchronization process only aims to synchronize the rotational speeds of the sleeve and the target gear ring. To eliminate the impacts between the sleeve and the gear ring, the angle alignment is introduced. Hence, the corresponding dynamic model for the synchronization process also should consider the angle difference, given by

$$\begin{aligned} \Delta\dot{\theta}_{\mathrm{gr\_slv}} &= \Delta\omega_{\mathrm{gr\_slv}} \\ \Delta\dot{\omega}_{\mathrm{gr\_slv}} &= \frac{1}{i_g}\frac{T_m}{J_{in}} \end{aligned} \tag{2}$$

where $\Delta\theta_{\mathrm{gr\_slv}} = \theta_{\mathrm{gr}} - \theta_{\mathrm{slv}}$ and $\Delta\omega_{\mathrm{gr\_slv}} = \omega_{\mathrm{gr}} - \omega_{\mathrm{slv}}$ denote the rotational angle difference and speed difference between the target gear ring and the sleeve, respectively, T_m is the drive motor torque.

In Eq. (2), the drive motor torque T_m depends on the three-phase current out of the MCU. It takes time to produce the desired three-phase current corresponding to the torque command T_{cmd}. That means the real motor torque T_m needs a torque response process to reach the torque command, which results in a gap between the real motor torque and the motor torque command. The gap has considerable influence on motor control performance, which is analyzed in Sec. 7. Therefore, it is necessary to take account of the torque response process when building the system model. However, it is hard to build a precise physical model to describe this process since the control algorithm in MCU is complicated and unknown to us. Hence, we first obtain the experimental results, then derive a proper mathematical model to fit this process.

3.1 Torque Response Process of the Drive Motor.

In this section, the experiment description is first given. Then, the model for the torque response process is derived through the experimental results analysis.

3.1.1 Experiment Description. In order to thoroughly investigate the transient characteristics of motor and its controller under a step-input torque command, a series of experiments are carried out. We first let the motor running on a constant torque (initial torque T_0 in Fig. 5) and a constant speed (initial speed), then give a certain step torque command (T_{cmd}) to the MCU, record the torque and speed signal of motor until it comes to the steady-state. In order to build a model facilitating to optimize trajectories in Sec. 5, the experiments are carried out with sets of different initial torques, different initial speeds, and different torque commands, shown in Table 1. The test rig for experiments is shown in Fig. 6, which contains a battery simulator of AeroVironment 900 as a power source, an MCU and a drive motor as the tested system, a mechanical transmission, a TCU of National Instrument PXI-1042Q, and a host computer. During the experiments, the gear is set to the neutral gear to obtain the same situation of the

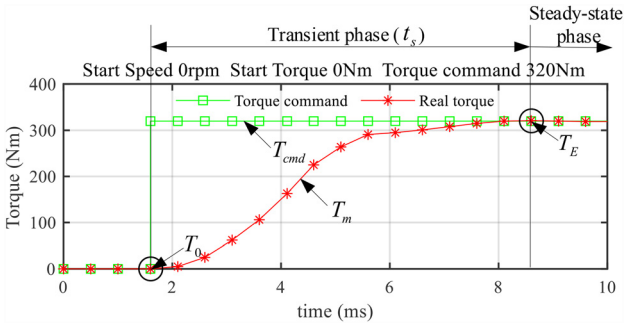

Fig. 5 An example of the drive motor torque response process

Table 1 Experiment variables

Variables	Scale	Unit
Initial speed	[0:100:1000]	rpm
Initial torque	[−400:40:400]	N·m
Torque command	[−400:40:400]	N·m

synchronization process. We assume that the MCU can calculate the drive motor torque T_m precisely, which means $\hat{T}_m = T_m$.

3.1.2 Results Analysis. Figure 5 shows a general example of the torque trajectory for the torque response process. It can be seen that the torque response process can be divided into two phases: (1) transient phase and (2) steady-state phase. It is easy to solve the motor torque in the steady-state phase with $T_m = T_E$. Besides that, it is necessary to build a model to describe the transient phase. We divide the solution of the transient phase model into two steps. First, the time t_s used for the transient phase is resolved. Then, the transient-phase model structure and parameters are chosen and derived.

The transient phase time t_s is potentially influenced by the initial speed, initial torque, and torque command since each experiment has different initial speeds, initial torques, and torque commands. We first analyze the effects of the initial speed on t_s. Figure 7 shows t_s almost stays unchanged with the increasing initial speed at different initial torques. That means the initial speed has little influence on t_s.

Then t_s only depends on the initial torque T_0 and torque command T_{cmd}. Figure 8 shows that t_s equals to zero when $T_{\mathrm{cmd}} = T_0$. When $|T_{\mathrm{cmd}} - T_0|$ increases, t_s rises piecewise linearly. Therefore, t_s can be regarded as a piecewise linear function of torque difference $T_{\mathrm{cmd}} - T_0$ approximately. To derive the function, we calculate the average transient phase time with same torque difference $T_{\mathrm{cmd}} - T_0$ and plot it along with different torque differences.

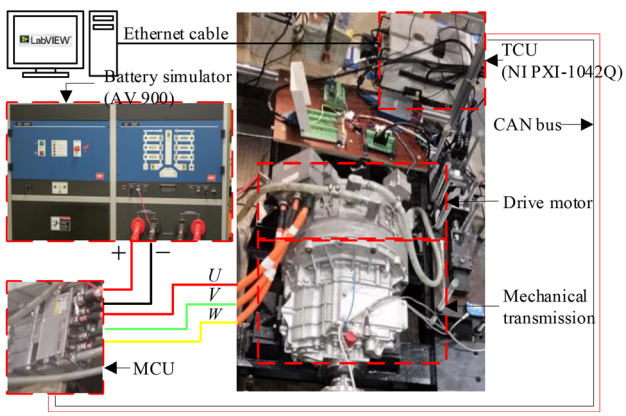

Fig. 6 Equipment diagram in experiments

Figure 9 shows the case in which both the initial torque and torque command are larger than or equal to zero, $T_0 \geq 0$ and $T_{\text{cmd}} \geq 0$. Furthermore, Figs. 9(*a*) and 9(*b*) show $T_{\text{cmd}} > 0$ and $T_{\text{cmd}} = 0$, respectively, since we find that the linear slope difference cannot be neglected in these two cases. We assume that the transient phase time is piecewise linear to the torque difference and the sign of the torque does not change during one torque switching process. Then when $T_{\text{cmd}} \geq 0$ and $T_0 \geq 0$, t_s can be given bywhen $T_{\text{cmd}} = 0$

$$t_s = \begin{cases} -0.0107T_{\text{diff}} + 0.617, & T_{\text{diff}} < -40 \quad (3a) \\ -0.0261T_{\text{diff}}, & T_{\text{diff}} \geq -40 \quad (3b) \end{cases}$$

when $T_{\text{cmd}} > 0$

$$t_s = \begin{cases} -0.0131T_{\text{diff}} + 1.827, & T_{\text{diff}} < -40 \quad (4a) \\ 0.0103T_{\text{diff}} + 1.939, & T_{\text{diff}} > 40 \quad (4b) \\ 0.0588|T_{\text{diff}}|, & |T_{\text{diff}}| \leq 40 \quad (4c) \end{cases}$$

where $T_{\text{diff}} = T_{\text{cmd}} - T_0$.

Similarly, when $T_{\text{cmd}} \leq 0$ and $T_m \leq 0$, t_s is calculated as:when $T_{\text{cmd}} = 0$

$$t_s = \begin{cases} 0.0109T_{\text{diff}} + 0.609, & T_{\text{diff}} > 40 \quad (5a) \\ 0.0261T_{\text{diff}}, & T_{\text{diff}} \leq 40 \quad (5b) \end{cases}$$

when $T_{\text{cmd}} < 0$

$$t_s = \begin{cases} -0.0106T_{\text{diff}} + 1.808, & T_{\text{diff}} < -40 \quad (6a) \\ 0.0125T_{\text{diff}} + 1.732, & T_{\text{diff}} > 40 \quad (6b) \\ 0.0558|T_{\text{diff}}|, & |T_{\text{diff}}| \leq 40 \quad (6c) \end{cases}$$

After the solution of t_s, the model structure and parameters are obtained in the following part. As shown in Fig. 5, the torque trajectory for the transient phase is an S-shaped curve. As an S-shaped model, delays added by the first-order model is a simple way to simulate the motor torque [28,29]. Sigmoid model is a typical S-shaped curve. These two typical S-shaped type curves are given by

Delay and first − order model:

$$T_m = T_0 + T_{\text{diff}}\left(1(t-\tau_d) - e^{-\left(\frac{t-\tau_d}{(t_s-\tau_d)/\tau_c}\right)}\right) \quad (7a)$$

Sigmoid model:

$$T_m = T_0 + \frac{T_{\text{diff}}}{1 + e^{-\frac{10}{t_s}\left(t - \frac{t_s}{2}\right)}} \quad (7b)$$

where τ_d denotes the time delay, and τ_c represents the time constant.

For a given experiment case, T_0 and T_{diff} are determined. Therefore, two parameters (τ_d and τ_c) need to be optimized for the delay

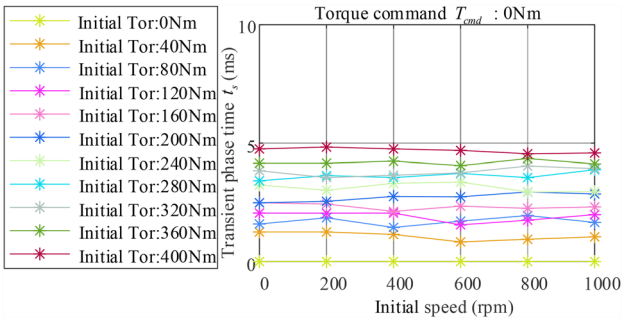

Fig. 7 Relationship between the transient phase time and the motor speed

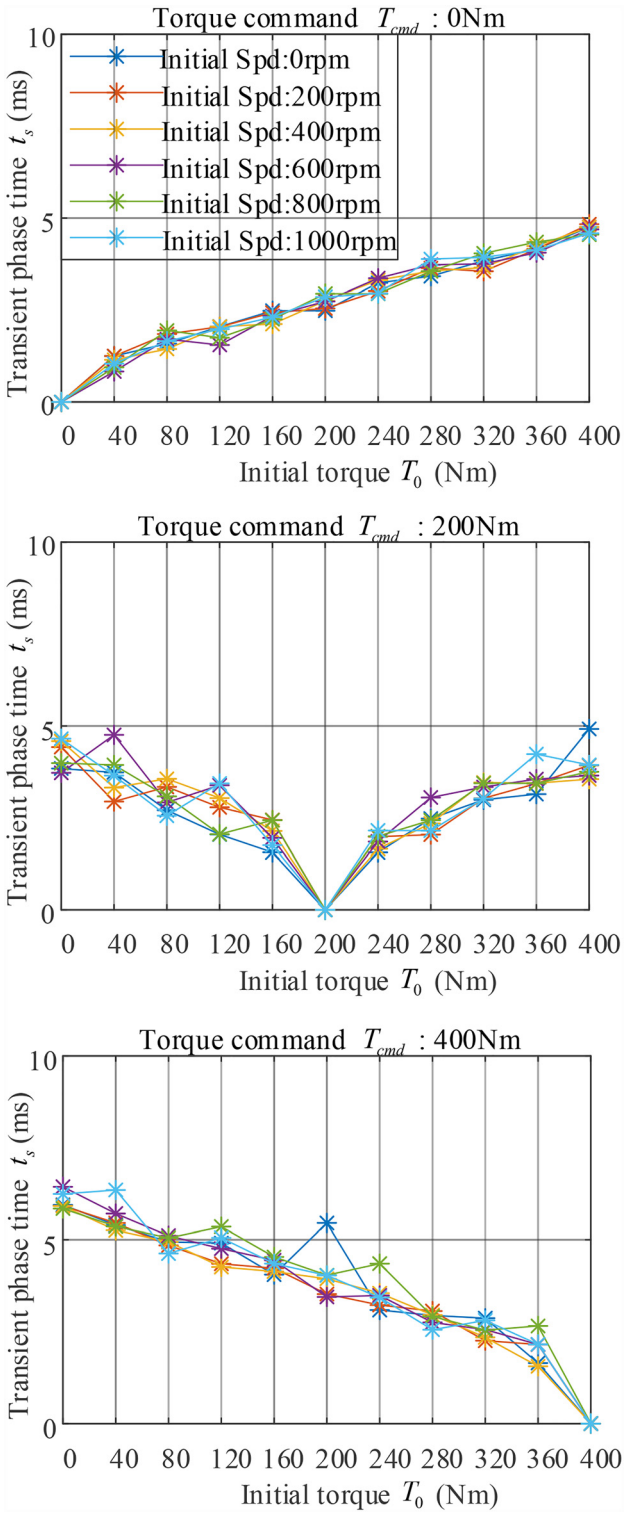

Fig. 8 Relationship between the transient phase time and the motor torque

and first-order model, while zero parameter for the Sigmoid model. After obtaining optimal parameters with genetic algorithm, a comparison between the delay and first-order model and Sigmoid model is achieved and shown in Fig. 10 and Table 2. Figure 10 and Table 2 show that the delay and first-order model can better fit the torque trajectory. However, the maximal error is a little large. Hence, we propose a modified Sigmoid model, given by

Modified Sigmoid model

$$T_m = T_0 + T_{\text{diff}}\left(x_5\left(t - \frac{t_s}{x_4}\right) + \frac{x_1}{1 + x_2 e^{\frac{x_3}{t_s}\left(t - \frac{t_s}{x_4}\right)}}\right) \tag{8}$$

where $x_j\,(j = 1, 2, \ldots, 5)$ denotes the parameters in modified Sigmoid model.

Figure 10 and Table 2 show the comparison among the three models. It can be seen that the modified Sigmoid model is more consistent with the experimental data but with more parameters. To obtain a precise result, we utilize the modified Sigmoid model.

Given the resolved t_s and modified Sigmoid model, the motor torque can be described as

$$T_m = \begin{cases} T_0 + T_{\text{diff}}\left(x_5\left(t - \frac{t_s}{x_4}\right) + \frac{x_1}{1 + x_2 e^{\frac{x_3}{t_s}\left(t - \frac{t_s}{x_4}\right)}}\right), & t \le t_s \\ T_0 + T_{\text{diff}}\left(x_5\left(t_s - \frac{t_s}{x_4}\right) + \frac{x_1}{1 + x_2 e^{\frac{x_3}{t_s}\left(t_s - \frac{t_s}{x_4}\right)}}\right), & t > t_s \end{cases} \tag{9}$$

4 Problem Formulation

According to the dynamic model for the synchronization process in Sec. 3, there exist command-based model parameters (t_s and $x_j\,(j = 1, 2, \ldots, 5)$) since these parameters change along with the torque command. Therefore, this is a multistage control problem.

For each stage, we should optimize not only the torque command T^i_{cmd} but also the time t^i_{ss} for the steady-state torque phase. Thus, the control policy includes a torque command array

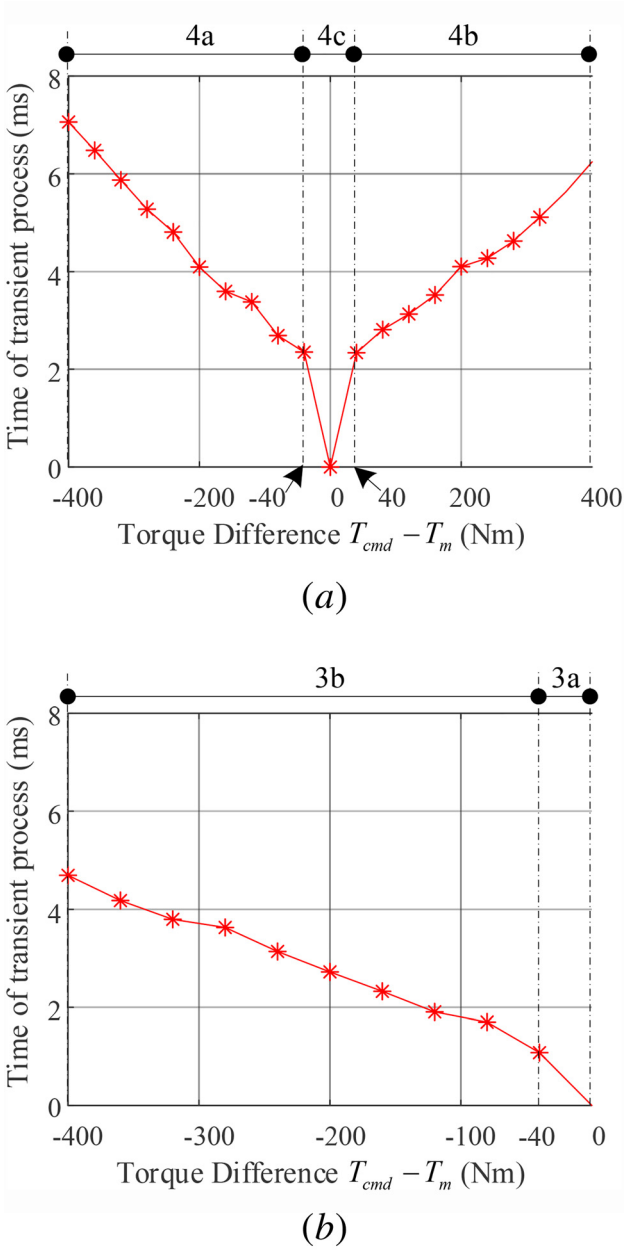

Fig. 9 Time of transient phase (t_s) varies with torque difference ($T_{\text{cmd}} - T_m$) (+→+, 0): (*a*) positive torque to positive torque (+→+) and (*b*) positive torque to zero torque (+→0)

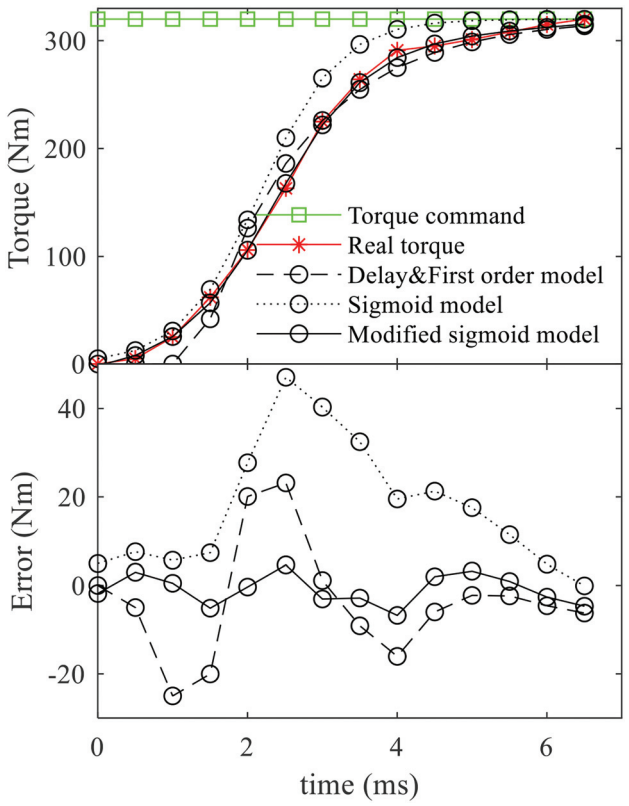

Fig. 10 A comparison example of the three model choices

Table 2 A comparison example of the three model choices

Model	NP	RSME	ME
Delay and First-order model	2	13.20 N·m	−25 N·m
Sigmoid model	0	22.55 N·m	47.00 N·m
Modified Sigmoid model	5	3.46 N·m	−6.76 N·m

NP, number of parameters optimized; RSME, root-square-mean error; and ME, maximal error.

$\mathbf{T_{cmd}} = [T^0_{\text{cmd}}, T^1_{\text{cmd}}, \ldots, T^{N-1}_{\text{cmd}}]^{\text{T}}$ and a steady-state time array $\mathbf{t_{ss}} = [t^0_{ss}, t^1_{ss}, \ldots, t^{N-1}_{ss}]^{\text{T}}$ $\mathbf{Zt_{ss}} = [t^0_{ss}, t^1_{ss}, \ldots, t^{N-1}_{ss}]^{\text{T}}$. T^i_{cmd} determines the time t^i_s and model parameters (x^i_j) for the transient phase. t^i_{ss} determines the time for the steady-state phase. The objective of the control problem is to minimize the total time during the synchronization process, which is the sum of the time t^i_s for transient phase and the time t^i_{ss} for the steady-state phase of all stages. That means this is a multistage time-optimal control problem, whose diagram is shown in Fig. 11. It can be summarized as

$$\min_{\mathbf{T_{cmd}}, \mathbf{t_{ss}}} J(\mathbf{T_{cmd}}, \mathbf{t_{ss}}) = \sum_{i=0}^{N-1} (t^i_s + t^i_{ss})$$

subject to constraints

The details for the objective function and constraints are given in the following.

4.1 Multistage Time-Optimal Control Problem. J, as the cost function, is the total time for the synchronization process. For a case given intial states T^0_m, $\Delta\omega^0_{\text{gr\_slv}}$, $\Delta\theta^0_{\text{gr\_slv}}$, and control policy $\mathbf{T_{cmd}}$, $\mathbf{t_{ss}}$, the cost function can be expressed as

$$J(T^0_m, \Delta\omega^0_{\text{gr\_slv}}, \Delta\theta^0_{\text{gr\_slv}}, \mathbf{T_{cmd}}, \mathbf{t_{ss}}) = \sum_{i=0}^{N-1} (t^i_s + t^i_{ss}) + t_{end}$$

Subject to:

Terminal conditions

$$\begin{cases} T^N_m = 0 \\ \Delta\omega^N_{\text{gr\_slv}} = 0 \\ \Delta\theta^N_{\text{gr\_slv}} = 0 \end{cases}$$

System dynamics:

State transition equation (details in Sec. 4.2)

Physical operation limits

$$\begin{cases} T^i_m \in [-T_{\max}, T_{\max}] \\ \Delta\omega^i_{\text{gr\_slv}} \in [\Delta\omega_{\text{gr\_slv\_min}}, \Delta\omega_{\text{gr\_slv\_max}}] \\ \Delta\theta^i_{\text{gr\_slv}} \in \left[0, \dfrac{2\pi}{N_{\text{gr}}}\right] \end{cases}$$

$$\begin{cases} T^i_{\text{cmd}} \in [-T_{\max}, T_{\max}] \\ t^i_{\text{ss}} \in [0, t_{\max}] \end{cases}$$

Initial conditions

$$\begin{cases} T^0_m = 0 \\ \Delta\omega^0_{\text{gr\_slv}} = \omega_0 \end{cases}$$

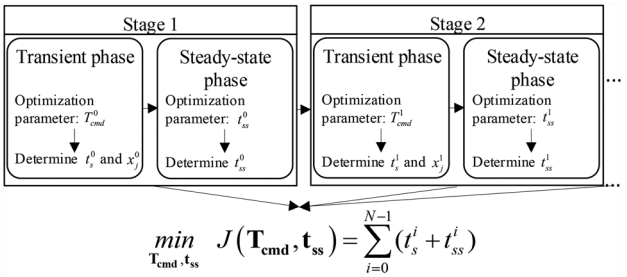

Fig. 11 Multistage time-optimal control problem diagram

where t_{end} in the cost function is introduced as a penalty to make sure that the optimal policy can not only achieve the aim of shortest time but also the desired final states. Thus, t_{end} depends on the final states, expressed as

$$t_{\text{end}} = \begin{cases} 0, T^N_m = 0\& \quad \Delta\omega^N_{\text{gr\_slv}} = 0\& \quad \Delta\theta^N_{\text{gr\_slv}} = 0 \\ \inf, \text{else} \end{cases} \tag{10}$$

Equation (10) means that the optimal policy should drive the motor torque, speed difference, and the angle difference to zeros at final stage since we expect zero motor torque, zero speed difference, and zero angle difference to eliminate the impacts between the sleeve and the gear ring, which are the terminal conditions in the above.

In addition, the states should also be constrained to the system dynamics which is summarized in a state transition equation in Sec. 4.2, the physical operation limits and the boundary conditions. The two control inputs should also subject to the physical operation limits

4.2 State Transition Equation. The system dynamics is summarized in a state transition equation in the following. To apply the DP algorithm in Sec. 5, the state transition equation needs to satisfy the nonaftereffect property. That is, future states are independent of past states given present states. To satisfy this prerequisite, the motor torque is introduced as another state besides of $\Delta\omega_{\text{gr\_slv}}$ and $\Delta\theta_{\text{gr\_slv}}$ because the motor torque depends on the initial torque T_0 at each stage. Moreover, we assume that the torque command does not change during the motor transient torque phase. Therefore, at each stage, the torque model includes both a transient phase and a steady-state phase. That means the motor torque reaches T_E at the end of one stage, and the total time for one stage is larger than the transient phase time t_s. Hence, based on the synchronization dynamic model in Eq. (2) and torque model in Eq. (9), the state transition equation is formulated as

$$\begin{bmatrix} T^{i+1}_m \\ \Delta\omega^{i+1}_{\text{gr\_slv}} \\ \Delta\theta^{i+1}_{\text{gr\_slv}} \end{bmatrix} = f^i(T^i_m, \Delta\omega^i_{\text{gr\_slv}}, \Delta\theta^i_{\text{gr\_slv}}, T^i_{\text{cmd}}, t^i_{ss}) \tag{11}$$

where T^i_m, $\Delta\omega^i_{\text{gr\_slv}}$, $\Delta\theta^i_{\text{gr\_slv}}$, and T^i_{cmd} are the motor torque, speed difference, angle difference and torque command at the *ith* stage , respectively, $\Delta\theta^i_{\text{gr\_slv}}$ is period-varied which can be seen in Eq. (12), t^i_{ss} represents the time for the steady-state phase, and f^i denotes the state transition function for stage i. f^i is

$$f^i = \left(\begin{bmatrix} 1 & 0 & 0 \\ \dfrac{1}{J_e} t^i_{ss} & 1 & 0 \\ \dfrac{1}{2J_e} t^i_{ss} 2 & t^i_{ss} & 1 \end{bmatrix} \begin{bmatrix} T^i_{m\_t^i_s} \\ \Delta\omega^i_{\text{gr\_slv}\_t^i_s} \\ \Delta\theta^i_{\text{gr\_slv}\_t^i_s} \end{bmatrix} \right) \text{mod} \begin{bmatrix} \inf \\ \inf \\ \dfrac{2\pi}{N_{\text{gr}}} \end{bmatrix} \tag{12}$$

where $T^i_{m\_t^i_s}$, $\Delta\omega^i_{\text{gr\_slv}\_t^i_s}$, and $\Delta\theta^i_{\text{gr\_slv}\_t^i_s}$ denote the motor torque, the speed difference, and angle difference at the end of the transient torque phase for stage i, given by

$$\begin{bmatrix} T^i_{m\_t^i_s} \\ \Delta\omega^i_{\text{gr\_slv}\_t^i_s} \\ \Delta\theta^i_{\text{gr\_slv}\_t^i_s} \end{bmatrix} = \begin{bmatrix} T^i_E \\ \Delta\omega^i_{\text{gr\_slv}} + \int_0^{t^i_s} \dfrac{T^i}{J_e} dt \\ \Delta\theta^i_{\text{gr\_slv}} + \Delta\omega^i_{\text{gr\_slv}} t^i_s + \int_0^{t^i_s} \int_0^t \dfrac{T^i}{J_e} d\tau dt \end{bmatrix}$$

where T^i and T^i_E denote the motor torque trajectory during the transient torque phase and the torque value at the end of the transient phase, respectively, given by

Table 3 Transmission parameters

Parameters	Value	Unit
Maximum motor torque ($T_{\max}$)	400	N·m
Initial speed difference ($\omega^0_{\text{gr\_slv}}, \omega_0$)	−209.47	rpm
Equivalent inertia (J_e)	1.0025	kgm/s^2
Teeth number of sleeve (N_{gr})	30	—
Transmission ratio (i_g)	4.01	—

$$T^i = T^i_m + T^i_{\text{diff}}\left(x^i_5\left(t - \frac{t^i_s}{x^i_4}\right) + \frac{x^i_1}{1 + x^i_2 e^{\frac{x^i_3}{t^i_s}\left(t - \frac{t^i_s}{x^i_4}\right)}}\right)$$

$$T^i_E = T^i_m + T^i_{\text{diff}}\left(x^i_5\left(t^i_s - \frac{t^i_s}{x^i_4}\right) + \frac{x^i_1}{1 + x^i_2 e^{\frac{x^i_3}{t^i_s}\left(t^i_s - \frac{t^i_s}{x^i_4}\right)}}\right)$$

where $T^i_{\text{diff}} = T^i_{\text{cmd}} - T^i_m$, t^i_s means the time for the transient torque phase, $x^i_j\,(j = 1, 2, \ldots, 5)$ are the parameters of the modified Sigmoid model at the ith stage.

5 Dynamic Programming

The DP is a good choice to solve the optimal control problem, especially for a multistage one. Therefore, we apply DP to derive the optimal control law. After the formulation of the multistage time-optimal control problem, the derivation of the optimal policy and the corresponding cost function based on DP algorithm is presented in the following.

The cost function obtained with the optimal policy solution can be represented as

$$J^*(T^0_m, \Delta\omega^0_{\text{gr\_slv}}, \Delta\theta^0_{\text{gr\_slv}}, \mathbf{T^*_{cmd}}, \mathbf{t^*_{ss}}) = \min_{\mathbf{T_{cmd}}, \mathbf{t_{ss}}} (t_{\text{end}} + \sum_{i=0}^{N-1}(t^i_s + t^i_{ss})) \tag{13}$$

The corresponding optimal policy is expressed as

$$\mathbf{T^*_{cmd}} = [T^{0*}_{\text{cmd}}, T^{1*}_{\text{cmd}}, \ldots, T^{N-1*}_{\text{cmd}}]^{\text{T}}$$
$$\mathbf{t^*_{ss}} = [t^{0*}_{ss}, t^{1*}_{ss}, \ldots, t^{N-1*}_{ss}]^{\text{T}} \tag{14}$$

To solve the optimal policy with the DP algorithm, the cost-to-go Y from control stage k to stage N is defined as

$$Y^*(T^{k-1}_m, \Delta\omega^{k-1}_{\text{gr\_slv}}, \Delta\theta^{k-1}_{\text{gr\_slv}}, k-1) = \min_{\mathbf{T_{cmd}}, \mathbf{t_{ss}}} (t_{\text{end}} + \sum_{i=k-1}^{N-1}(t^i_s + t^i_{ss})) \tag{15}$$

According to Bellman's principle, which is the basis of the DP algorithm, the cost-to-go can be updated backward as

$$Y^*(T^{k-1}_m, \Delta\omega^{k-1}_{\text{gr\_slv}}, \Delta\theta^{k-1}_{\text{gr\_slv}}, k-1) = \min_{T^{k-1}_{\text{cmd}}, t^{k-1}_{ss}} (t^{k-1}_s + t^{k-1}_{ss} + Y^*(f^{k-1}(T^{k-1}_m, \Delta\omega^{k-1}_{\text{gr\_slv}}, \Delta\theta^{k-1}_{\text{gr\_slv}}, T^{k-1}_{\text{cmd}}, t^{k-1}_{ss}), k)) \tag{16}$$

and the corresponding optimal control inputs at the *kth* stage can be solved as

$$[T^{k-1*}_{\text{cmd}}, t^{k-1*}_{ss}]^{\text{T}} = arg \min_{T^{k-1}_{\text{cmd}}, t^{k-1}_{ss}} (t^{k-1}_s + t^{k-1}_{ss} + Y^*(f^{k-1}(T^{k-1}_m, \Delta\omega^{k-1}_{\text{gr\_slv}}, \Delta\theta^{k-1}_{\text{gr\_slv}}, T^{k-1}_{\text{cmd}}, t^{k-1}_{ss}), k)) \tag{17}$$

Algorithm 1: An example of DP for N stages

Initialize states:
$T_{m\_vec} = -T_{max} : \delta T_m : T_{max}$;
$\Delta\omega_{gr\_slv\_vec} = \Delta\omega_{gr\_slv\_min} : \delta\omega : \Delta\omega_{gr\_slv\_max}$;
$\Delta\theta_{gr\_slv\_vec} = 0 : \delta\theta : \frac{2\pi}{N_{gr}}$;
Initialize control inputs:
$T_{cmd\_vec} = -T_{max} : \delta T_m : T_{max}$;
$t_{vec} = 0 : \delta t : t_{max}$;
Initialize index: $k = N$;
Initialize the cost-to-go at stage N:
for $T^N_m \in T_{m\_vec}, \Delta\omega^N_{gr\_slv} \in \Delta\omega_{gr\_slv\_vec}, \Delta\theta^N_{gr\_slv} \in \Delta\theta_{gr\_slv\_vec}$ **do**
  if $T^N_m = 0$ **and** $\Delta\omega^N_{gr\_slv} = 0$ **and** $\Delta\theta^N_{gr\_slv} = 0$ **then**
    $Y^*\left(T^N_m, \Delta\omega^N_{gr\_slv}, \Delta\theta^N_{gr\_slv}, N\right) = 0$
  else
    $Y^*\left(T^N_m, \Delta\omega^N_{gr\_slv}, \Delta\theta^N_{gr\_slv}, N\right) = inf$;
Compute the optimal control law:
while $k >= 0$ **do**
  $k = k - 1$;
  for $T^k_m \in T_{m\_vec}, \Delta\omega^k_{gr\_slv} \in \Delta\omega_{gr\_slv\_vec}, \Delta\theta^k_{gr\_slv} \in \Delta\theta_{gr\_slv\_vec}$ **do**
    Obtain the cost-to-go:
    $Y^*\left(T^k_m, \Delta\omega^k_{gr\_slv}, \Delta\theta^k_{gr\_slv}, k\right) = \min_{T^k_{cmd} \in T_{cmd\_vec}, t^k_{ss} \in t_{vec}} \left(t^k_s + t^k_{ss} + Y^*\left(f^k(T^k_m, \Delta\theta^k_{gr\_slv}, \Delta\omega^k_{gr\_slv}, T^k_{cmd}, t^k_{ss}), k+1\right)\right)$
    Obtain the optimal control inputs:
    $\left[T^{k*}_{cmd}, t^{k*}_{ss}\right]^T = arg \min_{T^k_{cmd} \in T_{cmd\_vec}, t^k_{ss} \in t_{vec}} \left(t^k_s + t^k_{ss} + Y^*\left(f^k(T^k_m, \Delta\theta^k_{gr\_slv}, \Delta\omega^k_{gr\_slv}, T^k_{cmd}, t^k_{ss}), k+1\right)\right)$
Result: Optimal policy:
$\mathbf{T^*_{cmd}} = \left[T^{0*}_{cmd}, T^{1*}_{cmd}, \ldots, T^{N-1*}_{cmd}\right]^T$ and
$\mathbf{t^*_{ss}} = \left[t^{0*}_{ss}, t^{1*}_{ss}, \ldots, t^{N-1*}_{ss}\right]^T$;
Optimal cost-to-go:
$J^*\left(T^0_m, \Delta\omega^0_{gr\_slv}, \Delta\theta^0_{gr\_slv}\right) = Y^*\left(T^0_m, \Delta\omega^0_{gr\_slv}, \Delta\theta^0_{gr\_slv}, 0\right)$

The parameters used in DP algorithm are shown in Table 3. The application of DP for N control stages is presented in the Algorithm 1. The corresponding solution diagram is shown in Fig. 12. Given a stage k, the states of the motor torque, the speed difference and the angle difference construct a three-dimension structure. The values of the states are shown in Table 4. For each point in the three-dimensional structure, we should solve the optimal control inputs, torque command T^{k*}_{cmd} and the optimal time t^{k*}_{ss}, and the corresponding cost-to-go $Y^*(T^k_m, \Delta\omega^k_{\text{gr\_slv}}, \Delta\theta^k_{\text{gr\_slv}}, k)$. The choices of T^k_{cmd} and t^k_{ss} are also shown in Table 4. To accelerate the computation, the high performance computing cluster in the Center for Computational Earth and Environmental Science at Stanford University is used to solve the dynamic programming. Eight nodes are used with sixteen cores in each node. Finally, it takes 12 h to solve the optimal policy for one control stage.

6 Rule-Based Control Strategy

In this section, the rule-based control strategy is extracted from DP results. Through analysis, a three-stage control strategy in normal operation situation and a four-stage control strategy in startup condition are derived, respectively, shown in a flowchart in Fig. 13. Normal operation means the situation in which the initial speed difference $\Delta\omega^0_{\text{gr\_slv}}$ is larger than 100 rpm. The recommended threshold value, 100 rpm, is determined by taking account of reducing the synchronization time and extending the applicable vehicle speed range. Startup condition is the situation in which the intial speed difference $\Delta\omega^0_{\text{gr\_slv}}$ equals to zero, whose corresponding vehicle speed also equals to zero. The following part presents the details of the rules' extraction in each situation.

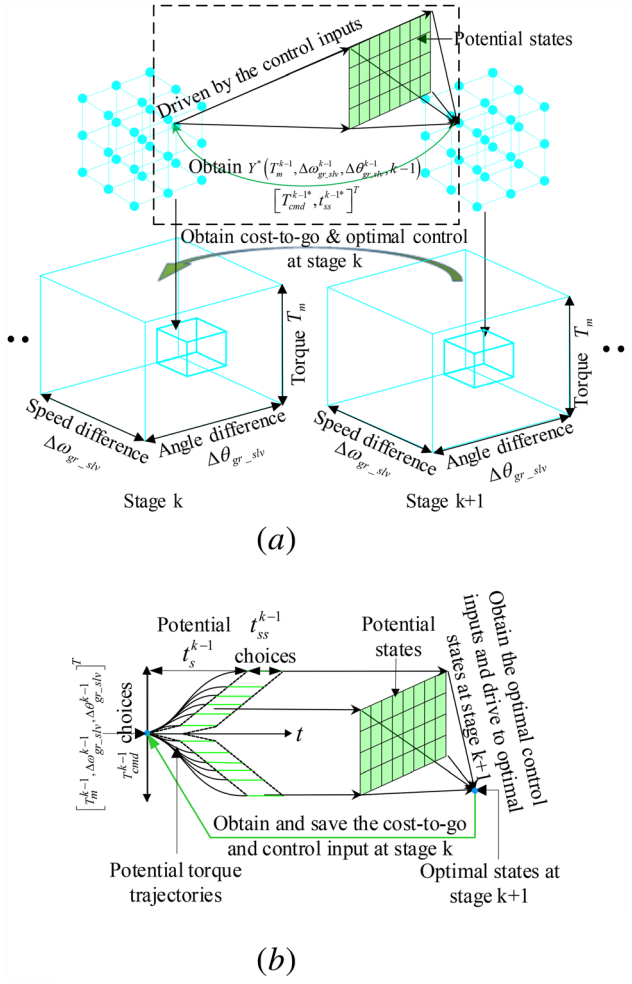

Fig. 12 DP backwards diagram: (*a*) DP backwards diagram and (*b*) details for the process in dotted box in (*a*)

Table 4 Variables and grids of the DP problem of downshifting from second gear to first gear

	Variables	Grid
Time	time (t_{ss}^k)	[0:0.0001:0.200] s
Control	Torque command (T_{cmd}^k)	[−400:1:400] N·m
States	Motor torque (T_m^k)	[−400:1:400] N·m
	Speed difference ($\Delta\omega_{\text{gr\_slv}}^k$)	[−310:1:50] rpm
	Angle difference ($\Delta\theta_{\text{gr\_slv}}^k$)	[0:0.02:12] deg

6.1 Rules for Normal Operation. To obtain the rule-based control strategy in the normal operation situation, the number of control stages is first analyzed. Then, the specific rules are described in analytic form.

First, we analyze the number of control stages. Figure 14(*a*) shows that the cost function varies with the changing number of control stage. It can be seen that the cost function decreases with the increase of the control stage. Beyond control stage three, the cost function reaches a plateau. Besides, there exists deviations during the solution of DP in each stage since we use discrete states with small intervals to replace the continuous states. Figure 14(*b*) shows that the root-square-mean error (RSME) increases with the increase of control stage. Taking these two main factors into consideration, three control stages seem to generate the best control choice.

Then, we derive the rules for normal operation. Figure 15 shows the motor torque trajectories at different initial angle differences $\Delta\theta^0_{\text{gr\_slv}}$. It can be seen that the motor torque begins at a low torque, then increases to pretty high torque near to the maximum limit of the motor, after that decreases to zero finally. Therefore, the optimal control rule can be summarized as follows: (1) starting at zero torque, (2) switching to the maximum torque, and (3) falling to zero. That means the torque commands for three stages are zero, maximum torque and zero, respectively, presented as

$$T^*_{\text{cmd}} = [0, -\text{sign}(\Delta\omega^0_{\text{gr\_slv}})T_{\max}, 0]^{\text{T}} \tag{18}$$

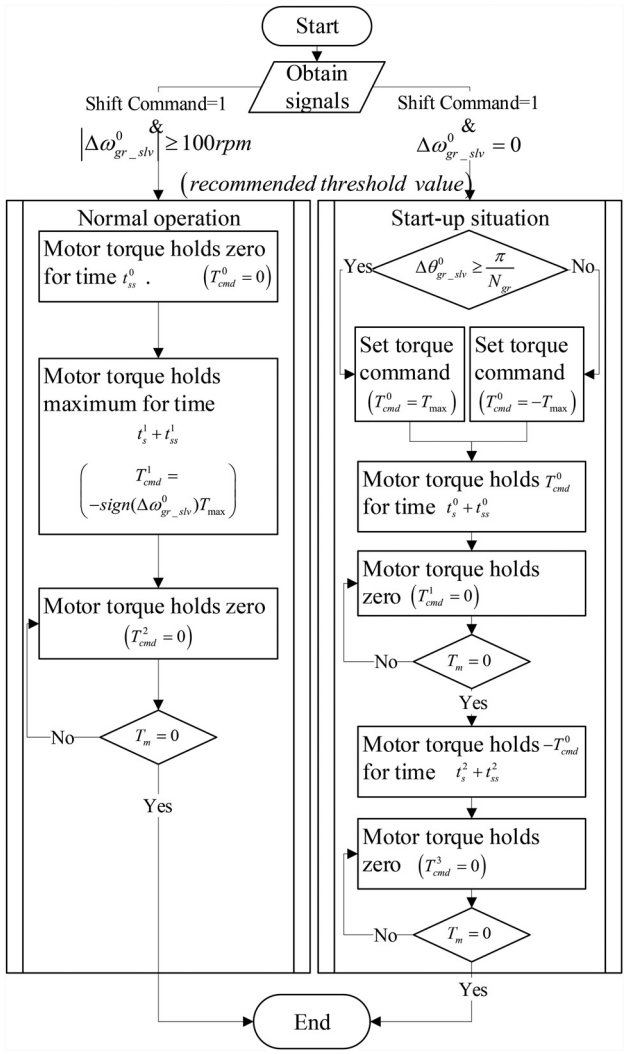

Fig. 13 Flowchart of the optimal rules

Thus, the torque command array is determined. As stated in Sec. 4, the steady-state time array $\mathbf{t}^*_{ss}$ also needs to be resolved besides of $\mathbf{T}^*_{cmd}$. As shown in Fig. 15, there is no steady-state phase at the third stage such that $t^2_{ss} = 0$. Therefore, there only remain two variables, t^0_{ss} and t^1_{ss}, that need to be calculated. These two variables can be solved based on the terminal conditions, $\Delta\omega^3_{gr\_slv} = 0$ and $\Delta\theta^3_{gr\_slv} = 0$. According to the state transition Eq. 17, it can be derived as

$$\Delta\omega^3_{gr\_slv} = \omega_0 - \text{sign}(\omega_0)\frac{T_{\max}}{J_e}t^1_{ss} + \sum_{i=1}^{2}\int_0^{t^i_s}\frac{T^i}{J_e}dt \tag{19}$$

$$\begin{aligned}\Delta\theta^3_{gr\_slv} = &\left(\theta_0 + \omega_0 t^0_{ss} + \omega_0 t^1_{ss} + \left(\int_0^{t^1_s}\frac{T^1}{J_e}dt\right)\left(t^1_{ss} + t^2_s\right)\right.\\ &+\sum_{i=1}^{2}\left(\omega_0 t^i_s + \int_0^{t^i_s}\int_0^{t}\frac{T^i}{J_e}d\tau dt\right)\\ &\left.-\text{sign}(\omega_0)\frac{T_{\max}}{2J_e}t^1_{ss}\left(t^1_{ss} + 2t^2_s\right)\right) \bmod \frac{2\pi}{N_{gr}}\end{aligned} \tag{20}$$

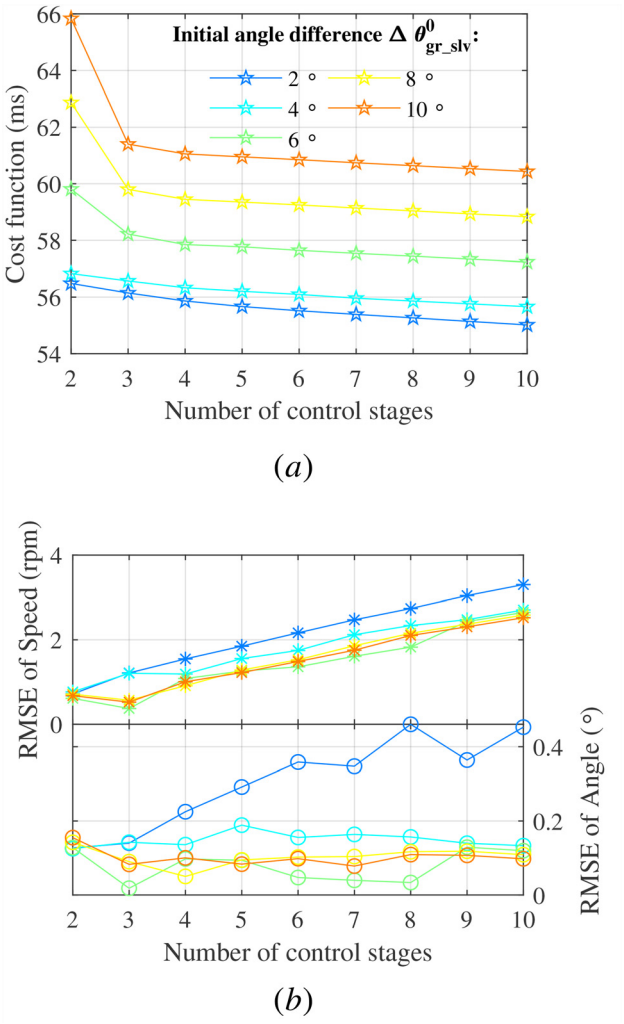

Fig. 14 Time cost and deviation at different initial angle differences $\Delta\theta_{gr\_slv}{}^0$ with different control stages in normal operation. RSME: root-square-mean error: (*a*) Cost function at different initial angle differences $\Delta\theta^0_{gr\_slv}$(2 deg : 2 deg : 10 deg) with different control stages and (*b*) speed and angle deviations at different initial angle differences $\Delta\theta^0_{gr\_slv}$(2 deg : 2 deg : 10 deg) with different control stages.

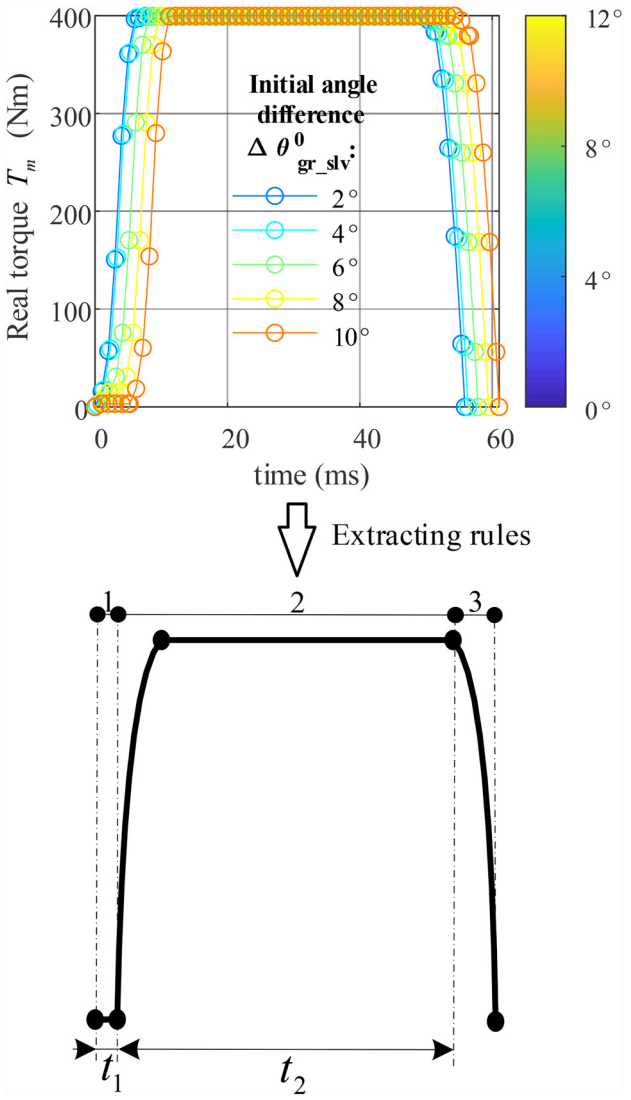

Fig. 15 The motor torque trajectories calculated by DP at different initial angle differences $\Delta\theta^0_{gr\_slv}$(2 deg : 2 deg : 10 deg) in normal operation

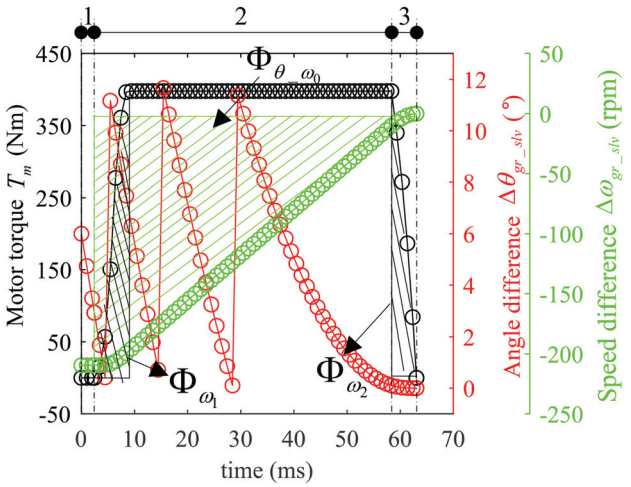

Fig. 16 One shifting case from second gear to first gear with initial angle difference equal to 6 deg in normal operation. Three lines represent trajectories of the motor torque, the speed difference, and the angle difference, respectively.

According to Eq. (19) and $\Delta\omega^3_{\text{gr\_slv}} = 0$, t^1_{ss} can be solved as

$$t^1_{ss} = \frac{J_e\omega_0 + \sum_{i=1}^{2}\int_0^{t^i_s} T^i dt}{\text{sign}(\omega_0)T_{\max}} \tag{21}$$

To further explain Eq. (21), one case in Fig. 16 is used to explain the notations. $\int_0^{t^i_s} T^i dt$ is substituted as Φ_{ω_i} shown in shaded regions in Fig. 16, which can reflect the speed synchronization during the transient torque phase. According to Eq. (20) and $\Delta\theta^3_{\text{gr\_slv}} = 0$, t^2_{ss} can be solved as:

$$t^0_{ss} = \begin{cases} \dfrac{(\theta_0 - \theta_0^{\text{pure}})}{-\omega_0}, (\theta_0 - \theta_0^{\text{pure}})\omega_0 \le 0 \\ \dfrac{\left((\theta_0 - \theta_0^{\text{pure}}) - \text{sign}(\omega_0)\dfrac{2\pi}{N_{\text{gr}}}\right)}{-\omega_0}, \text{else} \end{cases} \tag{22}$$

where $\theta_0^{\text{pure}} = \Phi_{\theta\_\omega_0} \bmod \frac{2\pi}{N_{\text{gr}}}$, $\Phi_{\theta\_\omega_0}$ denotes the angle alignments during stages 2 and 3, shown in the shaded regions in Fig. 16.

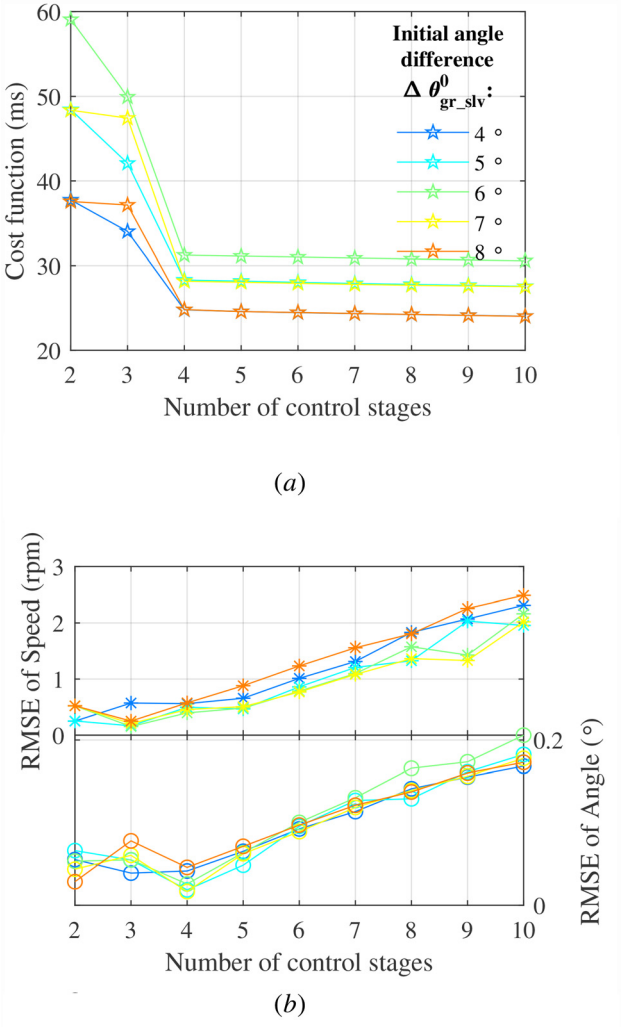

Fig. 17 Time cost and deviation at different initial angle differences with different control stages in startup situation. RSME: root-square-mean error: (*a*) time cost at different initial angle differences $\Delta\theta^0_{\text{gr\_slv}}$(4 deg : 1deg : 8 deg) with different control stages and (*b*) speed and angle deviations at different initial angle differences $\Delta\theta^0_{\text{gr\_slv}}$(4 deg : 1deg : 8 deg) with different control stages.

6.2 Rules for Startup Situation ($\Delta\omega^0_{\text{gr\_slv}}$=0). We discuss the optimal rules extracted for startup situation in this part. Similarly, the number of control stages is first analyzed. According to Fig. 17, four control stages seems to generate the best control choice.

Then, we can derive the rules according to the motor torque trajectories at different angle differences in Fig. 18. According to Fig. 18, the control rules can be summarized as: (1) increasing to the maximum torque, (2) then decreasing to zero, (3) after that, switching to the maximum torque in the opposite direction, and (4) finally falling into zero. Therefore, the torque commands for four stages can be presented as

$$\mathbf{T}^*_{\text{cmd}} = \begin{cases} [-T_{\max}, 0, T_{\max}, 0]^{\text{T}}, \theta_0 < \dfrac{\pi}{N_{\text{gr}}} \\ [T_{\max}, 0, -T_{\max}, 0]^{\text{T}}, \text{else} \end{cases} \tag{23}$$

According to Fig. 18, there is no steady-state phase at the first stage and the fourth stage. That means $t^1_{ss} = t^3_{ss} = 0$. Such that there only remain two variables, t^0_{ss} and t^2_{ss}, which can be determined based on the terminal conditions, $\Delta\omega^4_{\text{gr\_slv}} = 0$ and $\Delta\theta^4_{\text{gr\_slv}} = 0$. According to the state transition equation in Eq. (17), $\Delta\omega^4_{\text{gr\_slv}}$ can be derived as

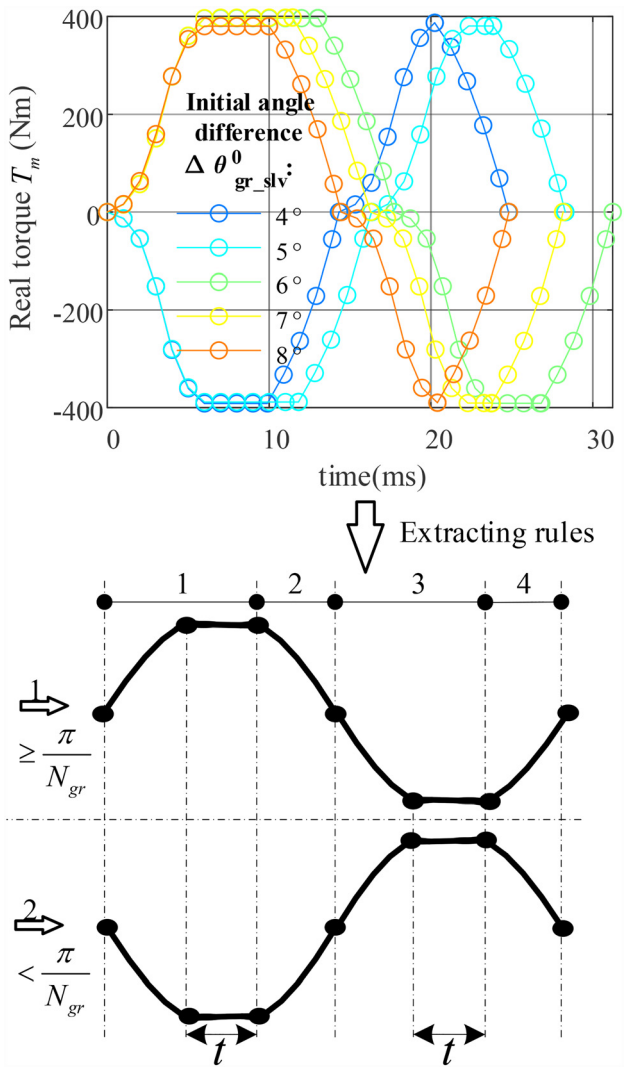

Fig. 18 The motor torque trajectories calculated by DP at different initial angle differences $\Delta\theta^0_{\text{gr\_slv}}$(4 deg : 1 deg : 8 deg) in startup situation

$$\Delta\omega^4_{\text{gr\_slv}} = \begin{cases} \dfrac{T_{\max}}{J_e}\left(t^2_{ss} - t^0_{ss}\right) + \displaystyle\sum_{i=0}^{3}\int_0^{t^i_s}(-1)^{i+1}\frac{T^i}{J_e}dt, \theta_0 < \dfrac{\pi}{N_{\text{gr}}} \\ \dfrac{T_{\max}}{J_e}\left(t^0_{ss} - t^2_{ss}\right) + \displaystyle\sum_{i=0}^{3}\int_0^{t^i_s}(-1)^{i}\frac{T^i}{J_e}dt, \text{else} \end{cases} \tag{24}$$

where $\sum_{i=0}^{3}\int_0^{t^i_s}(-1)^{i+1}\frac{T^i}{J_e}dt = 0$ and $\sum_{i=0}^{3}\int_0^{t^i_s}(-1)^{i}\frac{T^i}{J_e}dt = 0$ because the torque command is odd-symmetric with respect to the midpoint. Therefore, $t^0_{ss} = t^2_{ss}$ since $\Delta\omega^4_{\text{gr\_slv}} = 0$. Since the angle difference is is even-symmetric, then

$$\frac{\theta_0}{2} = \begin{cases} -\displaystyle\sum_{i=0}^{1}\int_0^{t^i_s}\int_0^{t}\frac{T^i}{J_e}d\tau dt + \frac{T_{\max}}{2J_e}t^0_{ss}\left(t^0_{ss} + 2t^1_s\right) \\ -\left(\displaystyle\int_0^{t^0_s}\frac{T^0}{J_e}dt\right)\left(t^0_{ss} + t^1_s\right), & \theta_0 < \dfrac{\pi}{N_{\text{gr}}} \\ \dfrac{\pi}{N_{\text{gr}}} - \left(\displaystyle\sum_{i=0}^{1}\int_0^{t^i_s}\int_0^{t}\frac{T^i}{J_e}d\tau dt + \frac{T_{\max}}{2J_e}t^0_{ss}\left(t^0_{ss} + 2t^1_s\right) + \left(\int_0^{t^0_s}\frac{T^0}{J_e}dt\right)\left(t^0_{ss} + t^1_s\right)\right), & \text{else} \end{cases} \tag{25}$$

where we use $\Phi_{\theta i}$ and Φ_ω to substitute $\int_0^{t^i_s}\int_0^{t}\frac{T^i}{J_e}d\tau dt$ and $\int_0^{t^0_s}T^0 dt$, , respectively, shown in the shaded regions of Fig. 19.

According to Eq. (25), t^0_{ss} can be derived as

$$t^0_{ss} = t^2_{ss} = \begin{cases} \dfrac{1}{T_{\max}}\left(\sqrt{\left(J_e\Phi_\omega - T_{\max}t^1_s\right)^2 + 2J_eT_{\max}C_\theta} + J_e\Phi_\omega - T_{\max}t^1_s\right), & \theta_0 < \dfrac{\pi}{N_{\text{gr}}} \\ \dfrac{1}{T_{\max}}\left(\sqrt{\left(J_e\Phi_\omega + T_{\max}t^1_s\right)^2 + 2J_eT_{\max}\left(\dfrac{\pi}{N_{\text{gr}}} - C_\theta\right)} - J_e\Phi_\omega - T_{\max}t^1_s\right), \text{else} \end{cases} \tag{26}$$

where $C_\theta = \Phi_{\theta_0} + \Phi_{\theta_1} + \Phi_\omega t^1_s + \frac{\theta_0}{2}$ for simplicity.

7 Results and Analysis

In this section, cases in both situations, normal operation situation and startup situation, are first studied. Then, to highlight the influence of the torque response process on the synchronization process, a comparative study with bang–bang control is taken since it is validated the bang–bang control is the optimal control law without considering the torque response process in Ref. [23]. Moreover, to further show the time-optimal property, comparisons with the pure speed synchronization control are also conducted.

7.1 Case Study. We first analyze one case of the synchronization process when shifting from 2nd gear to 1st gear in the normal operation situation. Figure 16 shows the trajectories of states during the synchronization process. As stated in Sec. 6.1, there are three control stages during the synchronization process. Accordingly, the trajectories of the states can also be divided into three stages. At the first stage, the torque remains zero. Therefore, the speed difference keeps constant, and angle alignment only depends on the speed difference. At the second stage, the changing of the speed difference and angle difference stays almost the same as that at the first stage during the transient torque phase. After the transient torque phase, the torque reaches the maximum and remains unchanged such that the speed difference decreases at the maximum rate. The angle difference varies slower and slower with the descending speed difference. At the last stage, the motor torque, speed difference, and angle difference change slowly to zero.

Then, one case of the synchronization process in the startup situation is shown in Fig. 19. As stated in Sec. 6.2, there are four control stages. At the first two stages, the motor torque first increases to the maximum torque then falls to zero. The speed difference increases to the peak point. In the last two stages, the motor torque increases to the maximum torque in the opposite

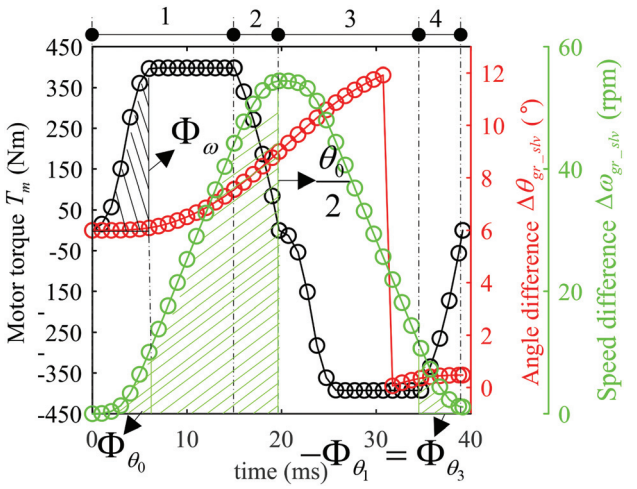

Fig. 19 An example out of the proposed rules with initial angle difference equal 6 deg in startup situation. Three lines represent trajectories of the motor torque, the speed difference, and the angle difference, respectively.

direction. The speed difference decreases to zero. During the four stages, the angle difference keeps decreasing and converges to zero finally.

Hence, the states can finally satisfy the terminal conditions with the proposed rules in both situations.

7.2 Comparison With Bang–Bang Control. The theoretical optimal control law for the synchronization process is resolved in Ref. [23] based on PMP without considering the torque response process. That means, in Ref. [23], it is assumed that the motor torque T_m can immediately reaches the torque commmand T_{cmd}. Finally, a bang-bang control is obtained in Ref. [23]. To analyze the influence of the torque response process on the synchronization performance, comparative case analysis is first made in normal operation situation and startup situation, respectively, shown in Fig. 20. We can see that the angle difference $\Delta\theta_{\text{gr\_slv}}$ and speed difference $\Delta\omega_{\text{gr\_slv}}$ driven by bang–bang control cannot satisfy the terminal conditions in both situations since the torque T_m cannot immediately achieve the torque command T_{cmd}.

To further compare the two methods, the synchronization time, the terminal speed difference, and the terminal angle difference with different initial angle difference $\Delta\theta^0_{\text{gr\_slv}}$ at $\Delta\omega_{\text{gr\_slv}} = -209.47$ rpm and $\Delta\omega_{\text{gr\_slv}} = 0$ rpm are calculated and shown in Fig. 21. We can see that the proposed rule has almost the same synchronization time as the bang–bang control. However, there are residual speed difference and angle difference with bang-bang control.

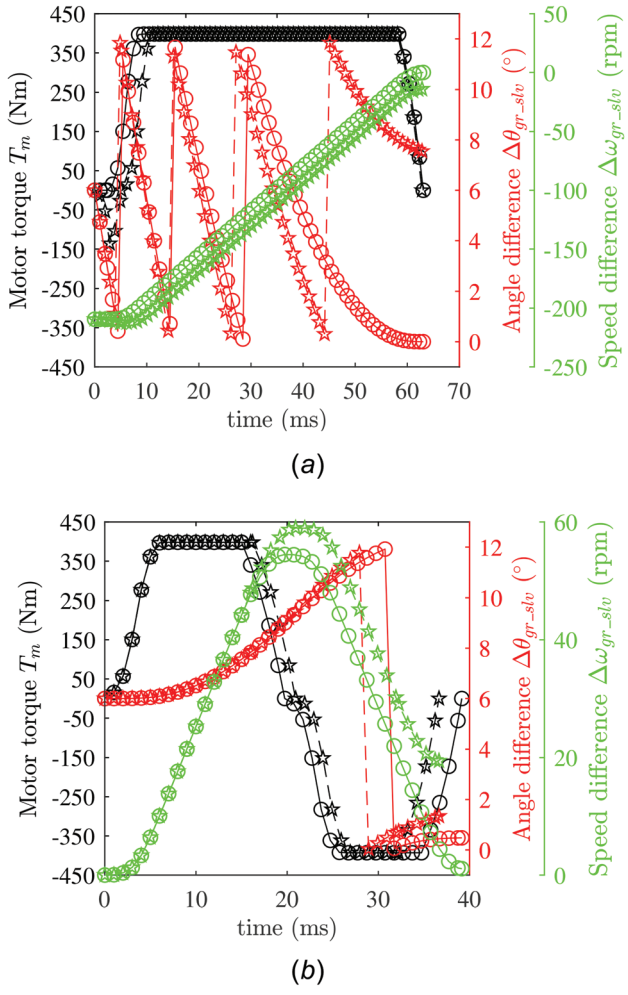

Fig. 20 (—○— (solid line) Dual synchronization with the proposed rules - - ☆ - - (dashed line) Bang-bang control) Comparisons between the proposed rules and the bang-bang control. Black, green, and red lines represent trajectories of the motor torque, the speed difference, and the angle difference, respectively: (*a*) normal operation situation and (*b*) startup situation.

7.3 Comparison With Pure Speed Synchronization. To further study the time-optimal property of the proposed rules, comparative research with pure speed synchronization control is taken in the following.

The comparative study is only conducted in normal operation situation since the pure speed synchronization control does not work in the startup situation with $\Delta\omega^0_{\text{gr\_slv}} = 0$. Figure 22(*a*) shows the trajectories of the states with the proposed rules and pure speed synchronization control. Compared with the pure speed synchronization, the proposed rules has one more stage, the first stage. In other words, the T_m trajectory of the pure speed synchronization coincides with the T_m trajectory out of the proposed

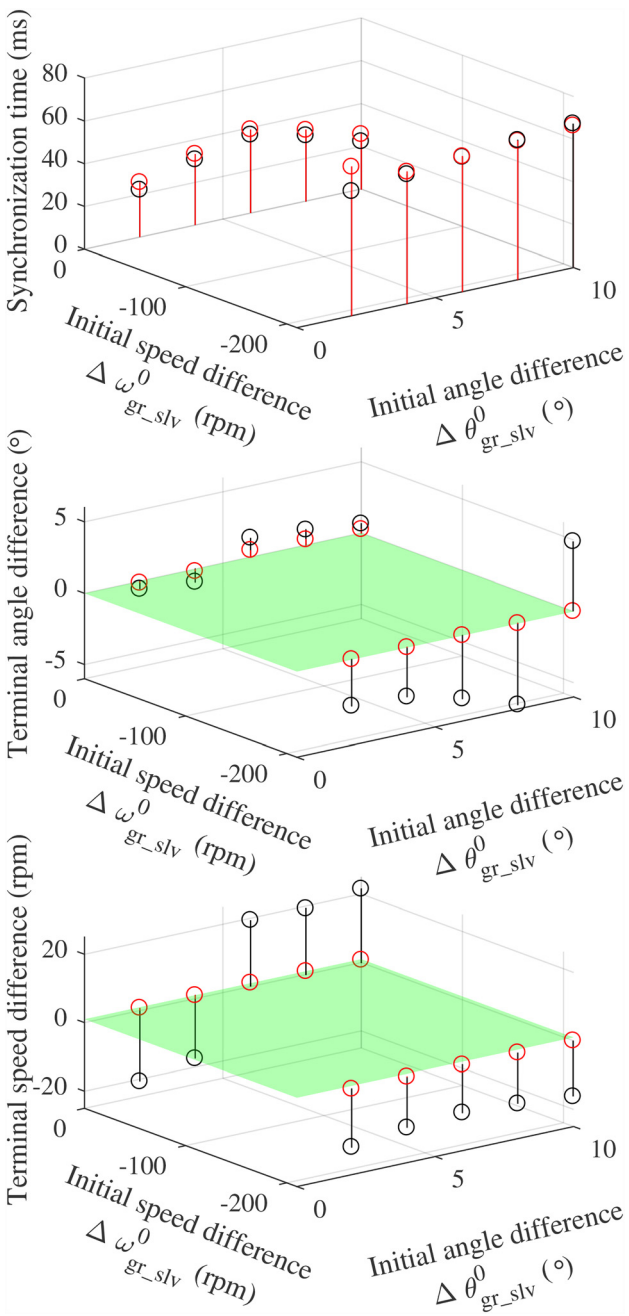

Fig. 21 (| Dual synchronization with the proposed rules, | Bang-bang control) Comparisons between the proposed rules and the bang-bang control

rule by a t_{ss}^0 translation. With the first stage, the angle difference $\Delta\theta_{\text{gr\_slv}}$ converges to zero finally, while that of pure speed synchronization does not equal to zero in the end.

To further analyze the reason why the angle difference can converge to zero with the proposed rule, the total alignment and the synchronization time for the synchronization process are shown in Fig. 22(*b*). It can be seen that when $\Delta\theta_{\text{gr\_slv}}^0 = \theta_0^{\text{pure}}$, the two methods have the same total angle alignment and synchronization time. That means $t_{ss}^0 = 0$ in this case such that the trajectories of states are the same with both methods. When $\Delta\omega_{\text{gr\_slv}}^0 > \theta_0^{\text{pure}}$, the total angle alignment has the same increment as that of initial angle difference $\Delta\theta_{\text{gr\_slv}}^0$. The corresponding synchronization time of the proposed rule also increases. That means the first control stage of the proposed rule is to align the angle difference equal to θ_0^{pure}. Therefore, the maximum synchronization time difference between the two methods is when the total angle alignment at first stage is one period $(2\pi/N_{\text{gr}})$. Then, the maximum synchronization time difference between the two methods can be easily solved as

$$\Delta t_{\text{rule\_pure}}^{\max} = \max(t_{\text{rule}} - t_{\text{pure}}) = \left|\frac{2\pi}{N_{\text{gr}}\omega_0}\right| \tag{27}$$

where t_{rule} and t_{pure} denote the synchronization time for the proposed rule and the pure speed synchronization, respectively.

Equation (27) also indicates that the maximum time difference decreases when the initial speed difference increases. The maximum time difference can be solved with respect to the recommended initial speed difference threshold, 100 rpm, which is 20 ms.

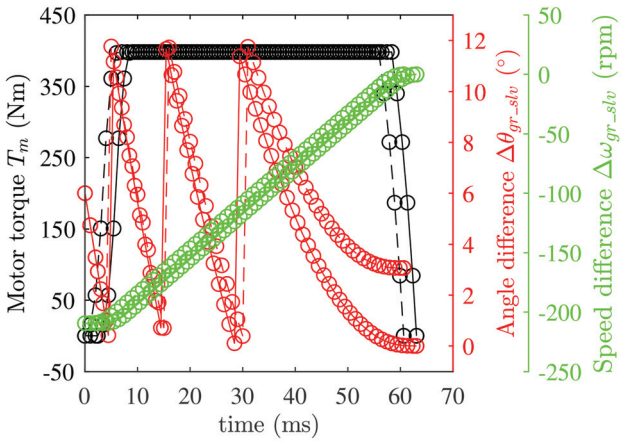

(*a*)

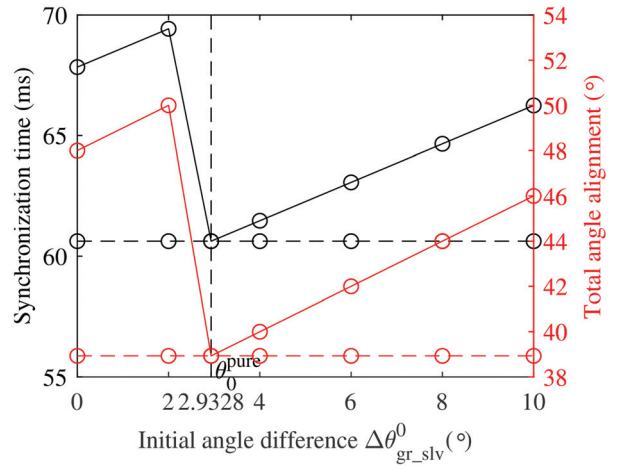

(*b*)

Fig. 22 (——⊖—— (solid line) Dual synchronization with proposed rules - - ⊖ - - Pure speed synchronization) Comparison between the proposed rules and pure speed synchronization in normal operation: (*a*) Comparison of the state's trajectories. Black, green, and red lines represent trajectories of the motor torque, the speed difference, and the angle difference, respectively and (*b*) comparison of time cost and angle difference accumulation. Black and red lines represent the time cost and the angle difference accumulation, respectively.

8 Conclusion

To avoid the impacts and better coincide with the practice, a time-optimal rule-based control strategy is proposed:

(1) A modified Sigmoid model is resolved, which can precisely depict the motor torque response process and facilitate the improvement of control accuracy.
(2) To solve the difficulty brought by command-based parameters in the modified Sigmoid model, the synchronization time-optimal control problem is converted to a multistage one and solved based on DP. According to the DP results, the rules are extracted as a three-stage rule strategy and a four-stage rule strategy in normal operation and startup situations, respectively.
(3) Considering the torque response process, the rule-based control strategy can make the angle difference and speed difference converge to zero simultaneously with almost the same time as that of bang-bang control. However, the bang-bang control cannot achieve zero terminals as it does not take account of the torque response process.

The current study did not consider the disturbances from the lubricant oil in the transmission and the resistances from the vehicle. Therefore, Future work includes designing the feedback control to improve the performance of the antidisturbance.

Acknowledgment

We would like to acknowledge the funding support of the National Natural Science Foundation of China (Grant No. 51775291), the China Scholarship Council (201806210156), and the computation resource support of Center for Computational Earth and Environmental Science at Stanford University.

Funding Data

- National Natural Science Foundation of China (Grant No. 51775291; Funder ID: 10.13039/501100001809).
- China Scholarship Council (Grant No. 201806210156; Funder ID: 10.13039/501100004543).

Nomenclature

T_{m} = torque out of the drive motor (N·m)
$T_{\max}$ = the maximum torque of the drive motor (N·m)
T_{cmd} = torque command for the drive motor (N·m)
T_0, T_E = the drive motor torque at the start point and the end point of the transient phase (N·m)
i_g = transmission ratio for the target gear
θ_m = rotational angle of the drive motor (rad)
θ_{gr} = rotational angle of the target gear ring, $\theta_{\text{gr}} = \frac{\theta_m}{i_g}$ (rad)
θ_{slv} = rotational angle of the sleeve (rad)
$\Delta\theta_{\text{gr\_slv}}$ = rotational angle difference between the target gear ring and the sleeve, $\Delta\theta_{\text{gr\_slv}} = \theta_{\text{gr}} - \theta_{\text{slv}}$ (rad)
Θ_0 = initial rotational angle difference between the target gear ring and the sleeve (rad)
ω_m = rotational speed of the drive motor (rad/s)
ω_{gr} = rotational speed of the target gear ring, $\omega_{\text{gr}} = \frac{\omega_m}{i_g}$ (rad/s)

ω_{slv} = rotational speed of the sleeve (rad/s)
$\Delta\omega_{gr\_slv}$ = rotational speed difference between the target gear ring and the sleeve, $\Delta\omega_{gr\_slv} = \omega_{gr} - \omega_{slv}$ (rad/s)
ω_0 = initial rotational speed difference between the target gear ring and the sleeve (rad/s)
J_{in} = equivalent inertia on the input shaft including all mechanisms connected to the input shaft of the transmission (kg m^2)
J_e = equivalent inertia on the target gear ring, which can be derived from J_{in}, $J_e = J_{in} i_g$ (kg m^2)
N_{gr} = number of teeth on the target gear ring or sleeve
x_j = parameters for the modified Sigmoid model ($j = 1, 2, \ldots, 5$)
t_s = time for the transient phase (s)
t_{rule} = synchronization time with the proposed rule (s)
t_{pure} = synchronization time with the pure speed synchronization control (s)

References

[1] Barton, B., and Schütte, P., 2017, "Electric Vehicle Law and Policy: A Comparative Analysis," J. Energy Natural Resour. Law, **35**(2), pp. 147–170.
[2] Kim, Y. H., 2014, "A Global Analysis and Market Strategy in the Electric Vehicle Battery Industry," Ph.D. thesis, Massachusetts Institute of Technology, Cambridge, MA.
[3] Yuan, Y., Wu, G., He, X., Song, Y., and Zhang, X., 2013, "Electric Vehicle Drivetrain Development in china," ASME Paper No. ISFA2012-7212.
[4] Eckert, J. J., Corrêa, F. C., Santiciolli, F. M., Costa, E. D S., Dionísio, H. J., and Dedini, F. G., 2016, "Vehicle Gear Shifting Strategy Optimization With Respect to Performance and Fuel Consumption," Mech. Based Des. Struct. Mach., **44**(1–2), pp. 123–136.
[5] Hailu, H. N., and Redda, D. T., 2018, "Design and Development of Power Transmission System for Green and Light Weight Vehicles: A Review," Open Mech. Eng. J., **12**(1), pp. 81–94.
[6] Socin, R. J., and Walters, L. K., 1968, "Manual Transmission Synchronizers," SAE Trans., **77**, pp. 31–65.
[7] Lovas, L., Play, D., Márialigeti, J., and Rigal, J.-F., 2006, "Mechanical Behaviour Simulation for Synchromesh Mechanism Improvements," Proc. Inst. Mech. Eng., Part D: J. Automobile Eng., **220**(7), pp. 919–945.
[8] Chen, H., Cheng, X., and Tian, G., 2016, "Modeling and Analysis of Gear-Shifting Process of Motor-Transmission Coupled Drive System," ASME J. Comput. Nonlinear Dyn., **11**(2), p. 021013.
[9] Chen, H., and Tian, G., 2016, "Modeling and Analysis of Engaging Process of Automated Mechanical Transmissions," Multibody Syst. Dyn., **37**(4), pp. 345–369.
[10] Fu, H., Tian, G., Chen, Y., and Chen, Q., 2009, "A Novel Control Scheme of Propulsion Motor for Integrated Powertrain of Electric Bus," 2009 IEEE Vehicle Power and Propulsion Conference, Dearborn, MI, Sept. 7–10, pp. 1496–1501.
[11] Falcone, F. J., Burns, J., and Nelson, D. J., 2010, "Closed Loop Transaxle Synchronization Control Design," SAE Technical Paper No. 2010-01-0817.
[12] Yu, H.-L., Xi, J.-Q., Zhang, F-Q., and Hu, Y-h., 2014, "Research on Gear Shifting Process Without Disengaging Clutch for a Parallel Hybrid Electric Vehicle Equipped With Amt," Math. Probl. Eng., **2014**, pp. 1–12.
[13] Yu, C.-H., Tseng, C.-Y., and Wang, C.-P., 2012, "Smooth Gear-Change Control for ev Clutchless Automatic Manual Transmission," 2012 IEEE/ASME International Conference on Advanced Intelligent Mechatronics (AIM), KaoHsiung, Taiwan, July 11–14, pp. 971–976.
[14] Tseng, C.-Y., and Yu, C.-H., 2015, "Advanced Shifting Control of Synchronizer Mechanisms for Clutchless Automatic Manual Transmission in an Electric Vehicle," Mech. Mach. Theory, **84**, pp. 37–56.
[15] Huang, J., Zhang, J., Huang, W., and Yin, C., 2018, "Optimal Speed Synchronization Control With Disturbance Compensation for an Integrated Motor-Transmission Powertrain System," ASME J. Dyn. Syst. Meas. Control, **141**(4), p. 041001.
[16] Mo, W., Walker, P. D., and Zhang, N., 2019, "Dynamic Analysis and Control for an Electric Vehicle With Harpoon-Shift Synchronizer," Mech. Mach. Theory, **133**, pp. 750–766.
[17] Mo, W., Wu, J., Walker, P. D., and Zhang, N., 2021, "Shift Characteristics of a Bilateral Harpoon-Shift Synchronizer for Electric Vehicles Equipped With Clutchless Amts," Mech. Syst. Signal Process., **148**, p. 107166.
[18] Laird, M., Lawton, B., and Gregory, R., 1990, "Dog Clutches for Rapid Gear Changes in Automotive Gearboxes," Proceedings of the Institution of Mechanical Engineers, First International Conference, Gearbox Noise and Vibrations, IMechE, Churchill College, University of Cambridge, Cambridge, UK, Apr. 9, pp. 103–112.
[19] Bóka, G., Lovas, L., Márialigeti, J., and Trencséni, B., 2010, "Engagement Capability of Face-Dog Clutches on Heavy Duty Automated Mechanical Transmissions With Transmission Brake," Proc. Inst. Mech. Eng., Part D: J. Automobile Eng., **224**(9), pp. 1125–1139.
[20] Duan, C., 2014, "Analytical Study of a Dog Clutch in Automatic Transmission Application," SAE Int. J. Passenger Cars-Mech. Syst., **7**(3), pp. 1155–1162.
[21] Lu, Z., Chen, H., Wang, L., and Tian, G., 2017, "The Engaging Process Model of Sleeve and Teeth Ring With a Precise, Continuous and Nonlinear Damping Impact Model in Mechanical Transmissions," SAE Technical Paper No. 2017-01-2443.
[22] Liu, H., Lei, Y., Li, Z., Zhang, J., and Li, Y., 2012, "Gear-Shift Strategy for a Clutchless Automated Manual Transmission in Battery Electric Vehicles," SAE Int. J. Commercial Veh., **5**(1), pp. 57–62.
[23] Lu, Z., Chen, H., Wang, L., and Tian, G., 2018, "Optimal Dual Synchronization Control of Rotational Speed and Angle in Non-Synchronizer Automatic Mechanical Transmission. Tech. rep," The 14th International Symposium on Advanced Vehicle Control, Beijing China, July 20.
[24] Piracha, M. Z., Grauers, A., Barrientos, E., Budacs, H., and Hellsing, J., 2019, "Model Based Control of Synchronizers for Reducing Impacts During Sleeve to Gear Engagement," SAE Paper No. 2019-01-1303.
[25] Piracha, M. Z., Grauers, A., and Hellsing, J., 2020, "Feedback Control of Synchronizers for Reducing Impacts During Sleeve to Gear Engagement," SAE Paper No. 2020-01-0960.
[26] Lu, Z., Tian, G., and Onori, S., 2020, "Time-Optimal Coordination Control for the Gear-Shifting Process in Electric-Driven Mechanical Transmission (Dog Clutch) Without Impacts," SAE Int. J. Elect. Veh., **9**(2), pp. 1–14.
[27] Biasini, R., Onori, S., and Rizzoni, G., 2013, "A near-Optimal Rule-Based Energy Management Strategy for Medium Duty Hybrid Truck," Int. J. Powertrains, **2**(2/3), pp. 232–261.
[28] Li, H., Yang, C., Hu, Y., Liao, X., Zeng, Z., and Zhe, C., 2016, "An Improved Reduced-Order Model of an Electric Pitch Drive System for Wind Turbine Control System Design and Simulation," Renewable Energy, **93**, pp. 188–200.
[29] Amornwongpeeti, S., Kiselychnyk, O., Wang, J., Shatti, N., Shah, N., and Soumelidis, M., 2017, "Adaptive Torque Control of IPMSM Motor Drives for Electric Vehicles," IEEE 26th International Symposium on Industrial Electronics (ISIE), Edinburgh International Conference Center in Scotland, Edinburgh, UK, June 19–21, pp. 226–231.